Reports of Practical Oncology and Radiotherapy 25 (2020) 507–514

Available online at www.sciencedirect.com

Reports of Practical Oncology and Radiotherapy

journal homepage: http://www.elsevier.com/locate/rpor

Original research article

Impact of acuros XB algorithm in deep-inspiration breath-hold (DIBH) respiratory techniques used for the treatment of left breast cancer

Lalit Kumar[a,b,*], Vimal Kishore[c], Manindra Bhushan[b], Abhinav Dewan[b], Girigesh Yadav[b], Kothanda Raman[b], Gourav Kumar[b], Irfan Ahmad[b], Kundan S. Chufal[b], Munish Gairola[b]

[a] Department of Applied Science & Humanities, Dr. A.P.J Abdul Kalam Technical University, Lucknow, India
[b] Medical Physics Division & Radiation Oncology Department, Rajiv Gandhi Cancer Institute and Research Center, New Delhi, India
[c] Department of Applied Science & Humanities, Bundelkhand Institute of Engineering & Technology, Jhansi, India

ARTICLE INFO

Article history:
Received 16 August 2019
Received in revised form 6 March 2020
Accepted 15 April 2020
Available online 27 April 2020

Keywords:
Acuros XB (AXB) algorithm
Deep inspiratory breathhold, low density medium, AAA

ABSTRACT

Aim: To investigate the impact of Acuros XB (AXB) algorithm in the deep-inspiration breath-hold (DIBH) technique used for treatment of left sided breast cancer.
Background: AXB may estimate better lung toxicities and treatment outcome in DIBH.
Materials and Methods: Treatment plans were computed using the field-in-field technique for a 6 MV beam in two respiratory phases - free breathing (FB) and DIBH. The AXB-calculations were performed under identical beam setup and the same numbers of monitor units as used for AAA-calculation.
Results: Mean Hounsfield units (HU), mass density (g/cc) and relative electron density were -782.1 ± 24.8 and -883.5 ± 24.9; 0.196 ± 0.025 and 0.083 ± 0.032; 0.218 ± 0.025 and 0.117 ± 0.025 for the lung in the FB and DIBH respiratory phase, respectively. For a similar target coverage ($p > 0.05$) in the DIBH respiratory phase between the AXB and AAA algorithm, there was a slight increase in organ at risk (OAR) dose for AXB in comparison to AAA, except for mean dose to the ipsilateral lung. AAA predicts higher mean dose to the ipsilateral lung and lesser V_{20Gy} for the ipsilateral and common lung in comparison to AXB. The differences in mean dose to the ipsilateral lung were 0.87 ± 2.66 % ($p > 0.05$) in FB, and 1.01 ± 1.07% ($p < 0.05$) in DIBH, in V_{20Gy} the differences were 1.76 ± 0.83% and 1.71 ± 0.82% in FB ($p < 0.05$), 3.34 ± 1.15 % and 3.24 ± 1.17 % in DIBH ($p < 0.05$), for the ipsilateral and common lung, respectively.
Conclusion: For a similar target volume coverage, there were important differences between the AXB and AAA algorithm for low-density inhomogeneity medium present in the DIBH respiratory phase for left sided breast cancer patients. DIBH treatment in conjunction with AXB may result in better estimation of lung toxicities and treatment outcome.

1. Background

Breast cancer is the most common cancer and leading cause for mortality among women worldwide; India along with the United States and China comprising almost one third of the global breast cancer burden.[1,2] Faced with an increasing incidence of breast cancer in metropolitan cities in India, it is anticipated that the need for modern radiotherapy for adjuvant treatment after breast cancer surgery will also increase proportionately. The IAEA has estimated that approximately 2500 teletherapy machines were installed and being used for treatment in developing countries till 1998. This figure is significantly below the estimated needs of almost 5000 machines at present and about 10,000 machines by the year 2015.[3] The Directory of Radiotherapy Centers (DIRAC) of IAEA checks in excess of 7600 radiotherapy centers, with around 15,600 machines (13,000 teletherapy and 2600 brachy-therapy units) serving the total populace around the glove. The DIRAC review shows a sensational disparity in the capacity of malignant growth patients to get to lifesaving radiotherapy across nations and districts of the world. In high income nations, one radiotherapy machine is accessible for each 120 000 individuals. In middle income nations, one machine serves more than 1 million individuals. In low income nations, around 5 million individuals depend upon a solitary radiotherapy machine.[4]

With the anticipated increase in demand, appropriate attention to RT dose calculation and delivery must be maintained to ensure

* Corresponding author at: Division of Medical Physics, Department of Radiation Oncology, Rajiv Gandhi Cancer Institute and Research Centre,Sector-5, Rohini, New Delhi 110085, India.
E-mail address: lalitk48@gmail.com (L. Kumar).

https://doi.org/10.1016/j.rpor.2020.04.011
1507-1367/

safe and effective radiotherapy practice. The International Commission on Radiation Units (ICRU) recommends an overall accuracy of up to 5% in the radiation dose delivered to a cancer patient.[5] Similar recommendations have also been proposed by the American Association of Physicists in Medicine (AAPM) in report no. 85,[6] which states that the uncertainty in dose distribution used to treat cancer must be less than 2%.

A number of studies have reported the limitations of dose calculation algorithms, such as analytical anisotropic algorithm (AAA), collapsed cone convolution (CCC) algorithm and pencil beam convolution (PBC) algorithm, in resolving dose delivered in an inhomogeneous medium.[7,8,9] Knoons et al.[10] and Fogliata et al.[11] have also reported that the dose calculation algorithms lacked accuracy in such media. Photon dose calculation is a challenging task as it depends on the mode of radiation interaction with a medium, photon energy and density of the encountered media. Accuracy of dose calculation algorithms is further complicated when confronting tissue with reduced density, such as in the case of the lung in deep-inspiration breath-hold (DIBH). Deviations and inaccuracies in dose calculation may have a profound impact on treatment outcomes.

Acuros XB (AXB) algorithm was developed by Transpire, Inc. (Gig Harbor, WA) from Attila[12] Attila is a general grid-based Boltzmann solvers (GBBS) code, which solves the differential form of the linear Boltzmann transport equation and is generalized for neutral, charged and coupled particle simulations.[13] Gifford et al.[14] and Vassiliev et al.[15] have described in detail the development of AXB. The AXB implementation in Eclipse TPS consists of two main components. The first one is the multiple source model, which is already implemented for the AAA algorithm in Eclipse. The other one is the radiation transport model. The AXB and AAA algorithms may differ substantially in tissues of differing atomic composition, density and homogeneity, such as soft tissue, lung and dense bony tissue. The AXB explicitly models the physical interactions of ionizing radiation with matter. In contrast, the AAA utilizes pre-calculated MC kernels scaled according to local density variations.

1.1. Aim

Impact of AXB on different clinical sites has been investigated in numerous studies.[16–20] Guebert et al.[21] assessed the clinical implementation of AXB for the right breast cancer patients treated using the DIBH technique and reported minimal difference in dose distribution between the AXB and AAA algorithm. Guebert et al.[21] has not stressed in detail the dosimetric difference in lung doses between the two algorithms. Fogliata et al.[22] reported the dosimetric impact of AXB for left breast cancer in free-breathing and DIBH with less number of cases compared to the present study. In this context, the present study aimed to evaluate the impact of the AXB algorithm for patients with left sided breast cancer being treated with the deep-inspiratory breath-hold (DIBH) technique. The present study analyzed the dosimetric parameters in terms of target volume coverage, organ-at-risk sparing, conformity and homogeneity index and integral dose to normal tissues. AXB calculated results were also compared against the AAA algorithm.

2. Materials and methods

2.1. Patient population, simulation and target delineation

Computed tomography (CT) data of 25 patients treated for left side breast carcinoma (10 with intact breasts and 15 with modified radical mastectomy) were randomly selected for this study. For all patients CT data sets were available in two different respiratory phases, viz. free breathing (FB) and amplitude gated deep inspiration breath hold (DIBH). Gating and respiratory tracking were evaluated by means of a Real-time Position Management™ (RPM) system (Varian Medical System, Palo Alto, USA). A Vac-Lok cushion was used for patient immobilization in a supine position with arms above the head. A radio opaque brass wire was kept around the breast surface for landmark identification as recommended by the consensus guidelines on target delineation.[23] All CT data sets were acquired on Siemens SOMATOM Sensation Open CT Scanner (Siemens Medical Systems, Germany). CT scans with slice thickness of 2 mm were acquired of the thorax region in scanning time of about 8 s.

For every patient, a single radiation oncologist performed contouring on both CT data sets. Planning target volume (PTV), and critical structures such as the ipsilateral, contralateral lung, common lung, contralateral breast, heart and spinal cord were contoured using a combination of automatic and manual segmentation tools available on the Eclipse TPS. Ipsilateral lung was divided into two sub-structures i.e.; Lung-IN, the volume of the lung falling inside the tangential field's projection as seen on beam's eye view (BEV) and Lung-OUT, the volume of lung outside the tangential field projection. Treatment planning was performed by a single medical physicist on both CT data sets. Treatment plans were computed using the field-in-field (FiF) technique based on tangential fields using 6 mega-volts (MV) photon beam energy from a Clinac-iX (2300CD) linear accelerator equipped with millennium multi leaf collimator (MLC). Millennium MLC consists of 60 leaf pairs with a resolution of 0.5 cm and 1.0 cm at the isocentre for inner 40 leaf pairs and outer 20 leaf pairs, respectively. Eclipse TPS version 11 (Varian Medical System, Palo Alto, USA) was used for treatment planning. A prescription dose (PD) was set to 50 Gy to the PTV in 25 fractions, at 2 Gy per fraction. Planning objective was to deliver 95% PD to 95% of the PTV with no more than 5% of PTV volume receiving 108% of PD.

2.2. Dose calculation

All the plans were calculated using the AAA version 11 and AXB version 11 algorithms (Varian Medical System, Palo Alto, USA) on Eclipse TPS. Grid resolution of 2.5 mm was used for dose calculation for both algorithms. The AXB calculations were performed under identical beam setup and the same numbers of monitor units (MUs), as used for AAA calculations. A dose-to-medium option was used for dose reporting in AXB calculations.

2.2.1. AAA

AAA is a pencil-beam convolution/superposition dose calculation algorithm. It uses a pre-defined Monte Carlo derived kernel to predict the tissue heterogeneity in the irradiation volume in which pencils are scaled with respect to equivalent path length in longitudinal distribution and lateral extension is scaled with density relative to water in normal directions by applying anisotropic independent exponential absorption functions. Further changes in lateral transport of energy are modeled when density varies in the irradiated volume. Two additional exponential functions are also utilized to further model the scaling with depth along the z-direction.[24,25]

2.2.2. AXB

The AXB depends on the explicit solutions of the Linear Boltzmann transport equation (LBTE) using deterministic numerical methods. The AXB models the physical interactions of ionizing radiation explicitly with tissue heterogeneity present in the irradiated volume. AXB provides the deterministic solution for the LBTE equation by direct discretization of the LTBE's variables into space, angle and energy.[26]

Table 1
Hounsfield Units (HUs), mass density and relative electron density at the levels of sternoclavicular joint, carina, and at 2 cm above the upper part of the diaphragm, for the lung in FB and DIBH respiratory phase, respectively.

Respiratory Phase	Parameters	Sternoclavicular	Carina	2 cm abovediaphragm	Average(Mean ± SD)
Free-breathing (FB)	Hounsfield Units (HU)	−757.5 ± 22.5	−779.1 ± 44.3	−809.8 ± 30.3	−782.1 ± 24.8
	Mass density (g/cc)	0.221 ± 0.023	0.199 ± 0.045	0.168 ± 0.030	0.196 ± 0.025
	Relative Electron density	0.243 ± 0.023	0.221 ± 0.044	0.190 ± 0.030	0.218 ± 0.025
Deep-breathing (DIBH)	Hounsfield Units (HU)	−860.4 ± 26.2	−895.2 ± 31.1	−894.8 ± 31.9	−883.5 ± 24.9
	Mass density (g/cc)	0.118 ± 0.026	0.083 ± 0.031	0.083 ± 0.032	0.083 ± 0.032
	Relative Electron density	0.140 ± 0.026	0.105 ± 0.031	0.105 ± 0.032	0.117 ± 0.025

Table 2
Dosimetric parameters for planning target volume calculated using AAA and AXB algorithms, in FB and DIBH respiratory phase, respectively.

Structure	DIBH			FB		
PTV	AAA	AXB	*p*-value	AAA	AXB	*p*-value
Mean (Gy)	51.18 ± 0.76	51.38 ± 0.73	0.113	51.65 ± 0.53	51.52 ± 0.58	0.106
$V_{90\%}$ (%)	98.53 ± 1.92	98.63 ± 1.98	0.566	98.64 ± 1.66	98.14 ± 1.84	0.065
$V_{95\%}$ (%)	96.62 ± 2.37	96.97 ± 1.96	0.261	96.10 ± 2.09	95.66 ± 2.37	0.152
$V_{108\%}$ (%)	0.61 ± 0.91	4.79 ± 4.35	0.015	1.15 ± 1.14	4.53 ± 2.30	0.001
Max (Gy)	53.83 ± 1.04	56.07 ± 0.99	0.000	54.84 ± 1.05	56.01 ± 0.54	0.012
HI	0.123 ± 0.090	0.129 ± 0.093	0.322	0.105 ± 0.076	0.113 ± 0.083	0.137
CI	1.322 ± 0.270	1.378 ± 0.318	0.036	1.409 ± 0.262	1.500 ± 0.318	0.004
NTID (liter-Gy)	62.30 ± 13.71	64.17 ± 13.98	0.000	59.67 ± 11.73	61.27 ± 12.02	0.000

2.3. Lung density evaluation

Lung density variations in two different respiratory phases (FB and DIBH) were realized using the Sector method.[27] Lung densities were calculated from the CT images in two different respiratory phases (FB and DIBH). Hounsfield Units (HU's) were measured at three levels: sternoclavicular joint, carina, and at 2 cm above the upper part of the diaphragm. HU of a pixel in CT image has an approximately linear relationship with the physical density of the tissue, comprised in the voxel.

Mass density was measured using the HU to mass density conversion calibration curve implemented in a treatment planning system.

Relative electron density was derived using the following formula:

$$\text{Relative electron density} = \left[\frac{\text{HU}}{1000}\right] + 1$$

2.4. Dosimetric evaluation

The dosimetric evaluation was performed by means of a standard dose-volume histogram (DVH). For PTV, evaluation was performed in terms of mean dose, $V_{90\%}$, $V_{95\%}$, and $V_{108\%}$. The plan dose homogeneity was evaluated using the homogeneity index (HI), defined as $(D_{2\%}\text{-}D_{98\%})/D_{50\%}$.[28] The plan dose conformity was evaluated using the conformity index (CI) defined as the 95% isodose volume relative to the size of the PTV.[29] For OARs, evaluation was performed in terms of mean dose and V_X values from the DVH, with X = 5, 10, 15, 20, 25, 30, 35, 40 and 45 Gy. Normal tissue integral dose (NTID) was also evaluated considering uniformity tissue density and defined as a product of mean dose and normal tissue volume outside the PTV.[30] A two sample paired *t*-test was used to compare the results. A *p*-value less than 0.05 was considered statistically significant with a 95% confidence limit.

3. Results

3.1. Evaluation of lung density

In DIBH phase, volumes of the left lung, right lung and common lung were increased by 1.9 ± 0.4, 1.7 ± 0.3 and 1.8 ± 0.3 times the volume in the FB phase. Lung characteristics for two different respiratory phases are listed in Table 1. The mean HU's were -782.1 ± 24.8 and −883.5 ± 24.9, mean mass density (g/cc) was 0.196 ± 0.025 and 0.083 ± 0.032, and relative electron density was 0.218 ± 0.025 and 0.117 ± 0.025, for the lung in FB and DIBH respiratory phases, respectively. Table 1 also shows that the HU's, mass density and relative electron density were lower at all anatomical levels (sternoclavicular joint, carina and 2 cm above the upper part of the diaphragm) in the lung for the DIBH respiratory phase, in comparison to the FB respiratory phase. In DIBH, the volume of the lungs increased due to air filling; therefore, density of the lung got reduced. Thus, HU's, mass density and relative electron density is lesser in the DIBH compared to FB respiratory phase.

3.2. Dosimetric evaluation

In the present study, 100 treatment plans of the 25 patients were analyzed. The dosimetric influence of the AXB algorithm in comparison to the AAA algorithm was studied for patients treated with the DIBH technique for left sided breast cancers. Clinically acceptable treatment plans were generated using forward-planned the field-in-field technique for the left breast in the FB and DIBH respiratory phases, respectively. The DVH curves show the difference between the AXB and AAA calculations for PTV and OARs (ipsilateral lung, lung-IN, lung-OUT) for a patient in Fig. 1 (a) for FB and Fig. 1 (b) for the DIBH respiratory phase, respectively. Fig. 2 shows the isodose distribution on axial planes in FB calculated using (a) AAA, (b) AXB, and in the DIBH respiratory phase calculated using (c) AAA, (d) AXB, respectively, for a case that well characterizes the examined group of patients. The dosimetric parameters for PTV coverage in the FB and DIBH respiratory phases, using AAA and AXB calculations are summarized in Table 2.

There were no significant differences in the target volume coverage and mean dose to the PTV ($p > 0.05$) in the FB and DIBH respiratory phase for the AXB and AAA calculated plans, respectively; however, a significant ($p < 0.05$) increase in $V_{108\%}$ and maximum dose in the FB and DIBH respiratory phase for the AXB plans in comparison to AAA calculated plans was observed. AXB-calculated plans were slightly inferior in terms of the conformity ($p < 0.05$) and homogeneity index ($p > 0.05$) in comparison to the AAA-calculated plans for the FB and DIBH respiratory phase, respectively. Integral dose to normal tissues (NTID) was significantly ($p < 0.05$) higher for

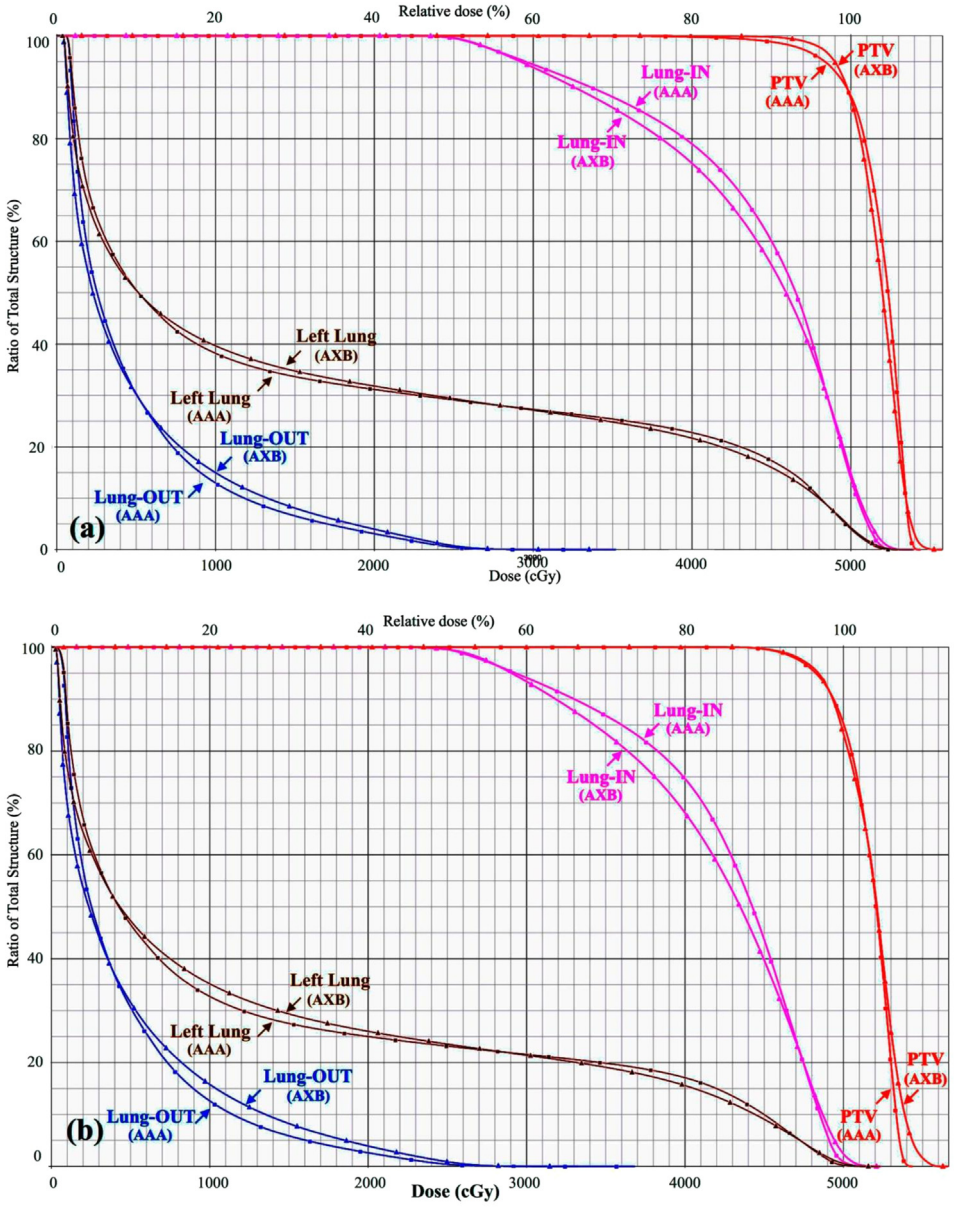

Fig. 1. Dose-volume histogram (DVH) for AXB and AAA calculated plan in for (a) free-breathing (FB) and (b) deep-inspiration breath-hold (DIBH) respiratory phase, respectively.

the AXB-calculation as compared to the AAA-calculated plans for both respiratory phases.

There was a slight increase in mean dose for the contralateral breast, contralateral lung, heart and spinal cord for the AXB-calculated plans in comparison to the AAA-calculated plans as shown in Table 3. In contrast, there was a reduction in mean dose to the ipsilateral lung, Lung-IN and Lung-OUT for both respiratory phases, except lung-IN in FB for the AXB-calculated plans in comparison to the AAA-calculated plans as shown in Table 3. The maximum dose differences between both the algorithms were $0.87 \pm 2.66\%$ ($p > 0.05$), $0.40 \pm 2.38\%$ ($p > 0.05$) and $6.43 \pm 3.08\%$ ($p < 0.05$) in the FB respiratory phase, $1.01 \pm 1.07\%$ ($p < 0.05$), $0.65 \pm 1.10\%$ ($p < 0.05$) and $1.76 \pm 2.80\%$ ($p < 0.05$) in the DIBH respiratory phase, for the ipsilateral lung, lung-IN and Lung-OUT, respectively.

There was a significant increase ($p < 0.05$) in V_{20Gy} for the ipsilateral lung and common lung in the FB and DIBH respiratory phase, respectively, for the AXB-calculated plans in comparison to the AAA-calculated plans. The maximum dose difference between both algorithms was $1.76 \pm 0.83\%$ and $1.71 \pm 0.82\%$ in the FB respiratory phase, $3.34 \pm 1.15\%$ and $3.24 \pm 1.17\%$ in the DIBH respiratory phase, for the ipsilateral and common lung, respectively. Fig. 3 demonstrated the difference between the AAA and AXB calculations in the lung region for the DIBH as compared to the the FB respiratory phase. There was a lager deviation found between the AAA and AXB calculation in the lung region for the DIBH compared to FB respiratory phase.

4. Discussion

The present study performs a dosimetric analysis to evaluate the dosimetric impact of AXB-calculations on the dose distribution for left sided breast cancer using a forward-planned FiF technique. Dose distribution analysis was performed using qualitative and quantitative techniques. The dosimetric data showed that there was no significant ($p > 0.05$) difference in coverage and mean dose

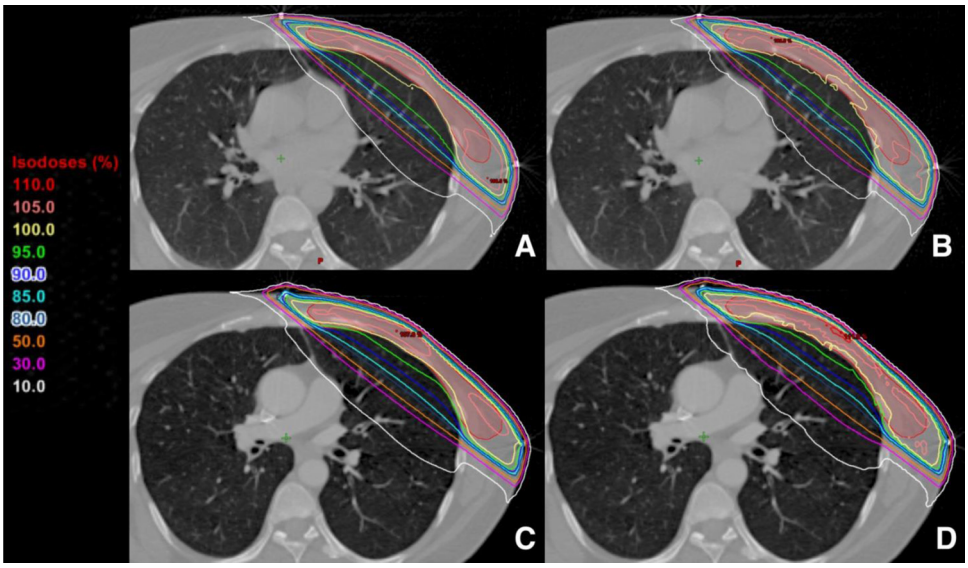

Fig. 2. Isodose distribution on axial planes in free-breathing (FB) calculated using (a) AAA, (b) AXB, and in deep-inspiration breath-hold (DIBH) respiratory phase calculated using (c) AAA, (d) AXB, respectively.

Table 3
Dosimetric parameters for OAR's calculated using AAA and AXB algorithms, in FB and DIBH respiratory phase, respectively.

Structure	DIBH			FB		
	AAA	AXB	*p*-value	AAA	AXB	*p*-value
Ipsilateral lung						
Mean (Gy)	10.54 ± 2.24	10.45 ± 2.31	0.001	10.69 ± 2.85	10.63 ± 2.91	0.279
V_{5Gy} (%)	36.88 ± 6.00	36.74 ± 5.95	0.280	35.51 ± 6.97	34.20 ± 7.21	0.000
V_{10Gy} (%)	25.21 ± 5.46	26.45 ± 5.52	0.000	24.72 ± 6.92	25.06 ± 7.11	0.000
V_{20Gy} (%)	18.96 ± 5.11	19.58 ± 5.13	0.000	19.36 ± 6.60	19.67 ± 6.63	0.000
V_{30Gy} (%)	16.06 ± 4.76	15.97 ± 4.77	0.000	16.39 ± 6.06	16.40 ± 6.06	0.505
V_{40Gy} (%)	11.98 ± 4.04	11.37 ± 4.14	0.000	12.48 ± 5.33	12.46 ± 5.28	0.751
V_{45Gy} (%)	6.72 ± 3.33	6.68 ± 3.41	0.801	8.15 ± 4.20	8.75 ± 4.34	0.003
Lung-IN						
Mean (Gy)	41.65 ± 1.23	41.38 ± 1.36	0.024	42.26 ± 1.29	42.43 ± 1.44	0.429
V_{30Gy} (%)	92.78 ± 1.76	92.47 ± 1.70	0.212	93.48 ± 1.15	93.41 ± 1.20	0.650
V_{35Gy} (%)	83.78 ± 3.34	81.19 ± 3.91	0.000	83.78 ± 3.44	83.20 ± 3.50	0.004
V_{40Gy} (%)	68.84 ± 5.99	64.85 ± 6.87	0.000	69.77 ± 6.78	69.64 ± 6.58	0.728
V_{45Gy} (%)	36.98 ± 12.09	36.74 ± 11.20	0.824	43.99 ± 11.31	47.40 ± 10.77	0.000
Lung-Out						
Mean (Gy)	3.97 ± 0.54	3.91 ± 0.56	0.016	3.87 ± 0.48	3.64 ± 0.51	0.000
V_{5Gy} (%)	23.52 ± 4.04	23.32 ± 3.88	0.208	21.52 ± 3.70	19.92 ± 3.78	0.000
V_{10Gy} (%)	9.46 ± 1.90	10.96 ± 2.19	0.000	8.50 ± 1.78	8.88 ± 2.11	0.002
V_{15Gy} (%)	4.51 ± 1.04	5.76 ± 1.23	0.000	4.38 ± 1.04	4.90 ± 1.23	0.000
V_{20Gy} (%)	2.03 ± 0.60	2.76 ± 0.68	0.000	2.08 ± 0.54	3.41 ± 4.18	0.182
V_{25Gy} (%)	0.37 ± 0.32	0.63 ± 0.35	0.000	0.37 ± 0.08	0.52 ± 0.12	0.000
Heart						
Mean (Gy)	3.30 ± 1.73	3.36 ± 1.40	0.088	5.85 ± 1.73	5.93 ± 1.70	0.001
V_{5Gy} (%)	8.35 ± 4.43	7.56 ± 4.29	0.000	16.31 ± 4.79	15.28 ± 4.70	0.000
V_{10Gy} (%)	4.26 ± 3.37	4.39 ± 3.42	0.004	10.30 ± 4.06	10.48 ± 4.09	0.000
V_{20Gy} (%)	2.98 ± 2.85	3.01 ± 2.86	0.004	8.22 ± 3.55	8.26 ± 3.52	0.273
V_{30Gy} (%)	2.27 ± 2.45	2.24 ± 2.42	0.026	7.02 ± 3.34	6.96 ± 3.29	0.004
Common lung						
Mean (Gy)	5.17 ± 1.05	5.19 ± 1.07	0.031	5.01 ± 1.32	5.04 ± 1.35	0.023
V_{5Gy} (%)	16.42 ± 4.91	16.35 ± 4.89	0.292	15.31 ± 4.11	14.79 ± 4.13	0.000
V_{10Gy} (%)	11.26 ± 3.68	11.82 ± 3.82	0.000	10.80 ± 3.41	10.95 ± 3.52	0.001
V_{20Gy} (%)	9.01 ± 2.29	9.29 ± 2.31	0.000	8.76 ± 2.98	8.90 ± 3.01	0.000
V_{30Gy} (%)	7.25 ± 2.76	7.17 ± 2.74	0.085	7.28 ± 2.73	7.28 ± 2.74	0.899
V_{40Gy} (%)	5.39 ± 2.21	5.13 ± 2.20	0.000	5.62 ± 2.37	5.60 ± 2.35	0.645
V_{45Gy} (%)	3.06 ± 1.64	3.04 ± 1.66	0.769	3.78 ± 1.90	4.03 ± 1.93	0.008
Contralateral breast						
Mean (Gy)	0.55 ± 0.28	0.91 ± 0.31	0.973	0.59 ± 0.57	0.94 ± 0.62	0.000
V_{5Gy} (%)	1.11 ± 1.07	1.24 ± 1.18	0.006	1.31 ± 1.99	1.47 ± 2.15	0.828
Contralateral lung						
Mean (Gy)	0.36 ± 0.11	0.47 ± 0.09	0.000	0.36 ± 0.12	0.50 ± 0.12	0.000
Spinal cord						
Mean (Gy)	0.30 ± 0.07	0.31 ± 0.07	0.168	0.27 ± 0.09	0.33 ± 0.11	0.000
D_{max} (Gy)	0.80 ± 0.19	0.79 ± 0.19	0.457	0.76 ± 0.35	0.86 ± 0.37	0.000

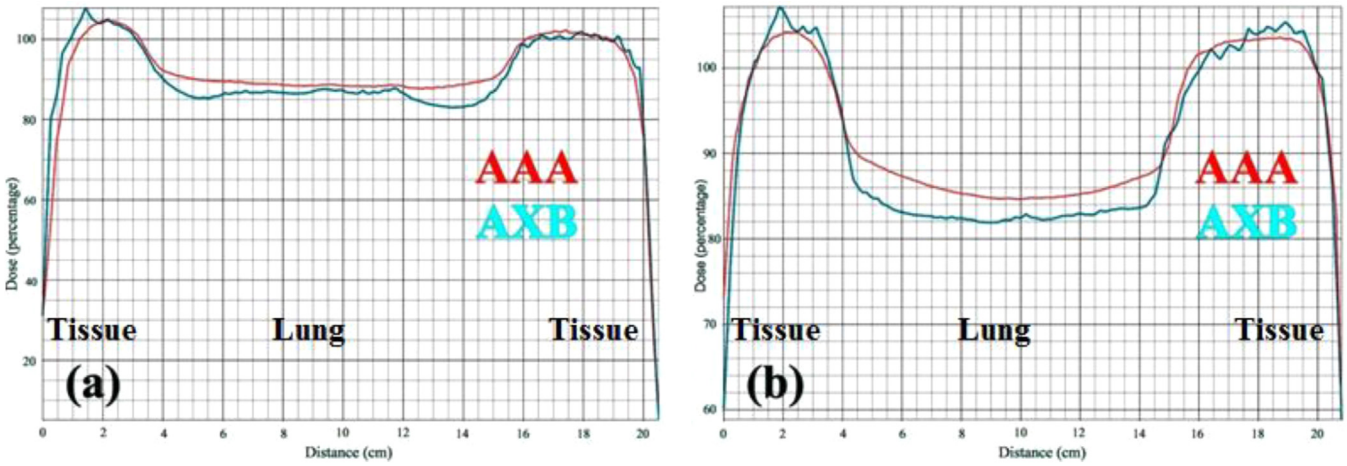

Fig. 3. Beam profile across the field edge for (a) free breathing and (b) deep inspiration breath-hold respiratory phases calculated using AAA and AXB algorithms.

to PTV, in the DIBH respiratory phase between the AAA and AXB algorithms. However, there was a significant increase in maximum dose and percentage volume of $V_{108\%}$ to PTV. Similarly, there was a slight increase in OAR's dose for the AXB-calculation in comparison to the AAA calculation, except for mean doses to the ipsilateral lung, lung-IN and lung-OUT ($p < 0.05$) in DIBH respiratory phase.

Present study reveals a significant difference in mean dose to the ipsilateral lung (1.01 ± 1.07 %) and lung-IN (0.65 ± 1.10%) and V_{20Gy} of the ipsilateral lung (3.34 ± 1.15%) between the AAA and AXB calculations in the DIBH respiratory phase. Foglita et al.[22] reported a significant dose difference of 1.5% for the lung region inside the field (lung-IN) in deep inspiration between the AXB version 10 and the AAA version 10 calculations. In the same study, Fogilata et al.[22] noted a significant dose difference of 1.3% for the lung region inside the field (lung-IN) while switching from the AXB version 10 to the AXB version 11, and concluded that AAA reported higher dose in comparison to the AXB algorithm, while accessing the capabilities of AXB algorithm in managing the inhomogeneity present in breast cancer.

Major differences were found in the dose received by the ipsilateral lung and its sub-volumes between both the algorithm calculations, which can be attributed largely to the change in lung density associated with different respiratory phases and methods employed for dose calculations. Lung density reduces in DIBH compared to FB due to air filling. In low-density lung tissue, range of secondary electrons increase due to reduced attenuation in the medium. This results in a large volume of electron disequilibrium and broadening of the penumbra at field boundaries. Hanley et al.[31] reported that penumbra increase should have a small clinical significance for DIBH using a 6 MV photon beam. In the DIBH respiratory phase, lateral electronic disequilibrium effect is more pronounced. Thus, adequate approximation of lateral electron transport in low-density medium (DIBH respiratory phase) is required to calculate the dose precisely. The difference in the dose between both algorithms depends upon the approximations made in the lateral electron transport, when density is very different from that of water. In low-density lung tissue, dose from the scattered electrons is deposited further away from the interaction point than that predicted by the correction based algorithm. This results in overestimation of dose in the high dose region (i.e. the percentage volumes of V_{30Gy}, V_{35Gy}, V_{40Gy} and V_{45Gy} for the Lung-IN region of the ipsilateral lung) and underestimation of dose in the low dose region of the lung (i.e. the percentage volumes of V_{10Gy}, V_{15Gy}, V_{20Gy} and V_{25Gy} for the Lung-OUT region of the ipsilateral lung) for the AAA algorithm in comparison to the AXB algorithm. In the DIBH respiratory phase with low lung density, the approximation made by AAA in the lateral electron transport appears insufficient to achieve accurate dose prediction in a low density lung. Therefore, lung volumes receiving low dose increase and volumes receiving high dose decrease for the AXB-calculations as compared to the AAA-calculated volumes.[32]

There is a difference in dose calculation approach between the AAA and AXB algorithms. The AXB calculates the dose to a medium by distinguishing between different types of body tissues characterized by significantly different chemical composition. In contrast to AAA, dose calculation accounts for the different densities of the material and the dose is computed as dose to density is rescaled to water. The accuracy of AXB has been investigated by many authors in a heterogeneous medium and reported comparable to gold standard Monte Carlo even in a low density medium.[11,33,34]

The irradiation of the heart and lung results in radiation induced side effects while delivering radiation therapy to the left breast. Radiation induced lung toxicities occur in the form of acute pneumonitis and sub-acute/late fibrosis. The risk of toxicity depends upon the total dose, dose per fraction and irradiated lung volume. Mean lung dose and lung volume receiving $\geq V_{20Gy}$ are the most commonly used parameters for accessing the risk of radiation induced lung toxicities.[35,36] V_{20Gy} less than 30% is the commonly used dose-volume criterion for minimizing the pneumonitis risk to the ipsilateral lung in left breast irradiation.[37] In the present study, V_{20Gy} was within the prescribed limits for both respiratory phases using both of the dose calculation algorithms. However, for DIBH, the present study showed significant ($p < 0.05$) reduction in mean dose to the ipsilateral lung, lung-IN and significant ($p < 0.05$) increase in V_{20Gy} for the ipsilateral and common lung using AXB calculations in comparison to AAA. Dose calculations algorithms are always an influencing factor in the assessment of lung toxicities. Therefore, the above differences may influence the treatment outcome and cannot be left unnoticed. Rana et al.[38] and Kathirvel et al.[39] have reported that AAA underestimates V_{20Gy} for the ipsilateral and common lung in comparison to AXB in their studies based on the appraisal of calculation accuracy of AXB and AAA in the thoracic region. The difference between AXB and AAA in calculating the V_{20Gy} for the ipsilateral and common lung may lead to the misinterpretation of the correlations between dose-volume levels and pre-defined toxicity for tissues, especially for low density lung tissues in the DIBH respiratory phase. As an extension of the present analysis, we are

currently evaluating the impact of these differences on the normal tissue complication probability associated with breast radiotherapy.

Major drawback of the present study was the limited number of patients and its reliance on the dosimetric data rather than clinical follow up. However, this study carefully investigates the impact of AXB calculation on the left breast cancer using the DIBH technique and gives an approximation of apossible clinical advantage of using AXB calculation for the DIBH technique.

5. Conclusion

The present study indicates that for similar target volume coverage, there were important differences between the AXB and AAA algorithm for low-density inhomogeneity medium present in the DIBH respiratory phase for left sided breast cancer patients. DIBH treatment in conjunction with AXB may result in better estimation of lung toxicities and treatment outcome.

Funding

None.

Conflict of interest

None.

Financial disclosure

None.

Acknowledgements

The authors thank the management of Rajiv Gandhi Cancer Institute & Research Centre in New Delhi, India for their continued support and encouragement to complete this research work.

References

1. Ferlay J, Soerjomataram I, Dikshit R, et al. Cancer incidence and mortality worldwide: Sources, methods and major patterns in GLOBOCAN 2012. *Int J Cancer*. 2015;136:E359–86.
2. Ferlay J, Shin HR, Bray F, Forman D, Mathers C, Parkin DM. Estimates of worldwide burden of cancer in 2008:GLOBOCAN 2008. *Int J Cancer*. 2010;127:2893–2917.
3. Radiation protection in the design of radiotherapy facilities, International Atomic Energy Agency Vienna, 2006 Safety Report Series No.47.
4. International Atomic Energy Agency. *Radiotherapy in Cancer care: Facing the global challenge*. Vienna: IAEA; 2017.
5. International Commission on Radiation Units and Measurements (ICRU). *Determination of absorbed dose in a patient irradiated by beams of X or gamma rays in radiotherapy procedures. ICRU Report 24*. Washington, DC: ICRU; 1976:67.
6. Papanikolau N, Battista JJ, Boyer AL, et al. *Tissue inhomogeneity corrections for megavoltage photon beams. Report of task group No. 65 of the radiation therapy committee of the american association of physicist in medicine. AAPM report No. 85*; 2004.
7. Gagné IM, Zavgorodni S. Evaluation of the analytical anisotropic algorithm in an extreme water-lung interface phantom using Monte Carlo dose calculations. *J Appl Clin Med Phys*. 2006;8(1):33–46.
8. Gray A, Oliver LD, Johnston PN. The accuracy of the pencil beam convolution and anisotropic analytical algorithms in predicting the dose effects due to attenuation from immobilization devices and large air gaps. *Med Phys*. 2009;36(7):3181–3191.
9. Oyewale S. Dose prediction accuracy of collapsed cone convolution superposition algorithm in a multi-layer inhomogeneous phantom. *Int J Cancer Ther Oncol*. 2013;1(1):01016.
10. knoos T. et al. Comparison of dose calculation algorithms for treatment planning in external photon beam therapy for clinical situations. Phys. Med. Biol. 51 5785-5807.
11. Fogliata A, Vanetti E, Albers D, et al. On the dosimetric behavior of photon dose calculation algorithms in the presence of simple geometric heterogeneities: Comparison with Monte Carlo calculations. *Phys Med Biol*. 2007;52(5):1363–1385.
12. Wareing TA, McGhee JM, Morel JE, Pautz SD. Discontinuous finite element Sn methods on three dimensional unstructured grids Nucl. *Sci. Eng*. 2001;138:256–268.
13. Lewis EE, Miller WF. *Computational methods of neutron transport*. New York: Wiley; 1984.
14. Gifford K, Horton J, Wareing T, Failla G, Mourtada F. Comparison of a finite-element multigroup discrete ordinates code with Monte Carlo for radiotherapy calculations. *Phys Med Biol*. 2006;51:2253–2265.
15. Vassiliev O, Wareing T, Davis I, McGhee J, Barnett D, Horton J, Gifford K, Failla G, Titt U, Mourtada F. Feasibility of a multigroup deterministic solution method for three-dimensional radiotherapy dose calculations. *Int J Radiat Oncol Biol Phys*. 2008;72:220–227.
16. Kan MW, Leung LH, Yu PK. Dosimetric impact of using the Acuros XB algorithm for intensity modulated radiation therapy and RapidArc planning in nasopharyngeal carcinomas. *Int J Radiat Oncol Biol Phys*. 2013;85(1):e73–80.
17. Pokhrel D, Sood S, Badkul R, et al. Assessment of Monte Carlo algorithm for compliance with RTOG 0915 dosimetric criteria in peripheral lung cancer patients treated with stereotactic body radiotherapy. *J Appl Clin Med Phys*. 2016;17(3):277–293.
18. Kim KH, Chung JB, Suh TS, et al. Dosimetric and radiobiological comparison in different dose calculation grid sizes between Acuros XB and anisotropic analytical algorithm for prostate VMAT. *PLoS One*. 2018;13(11):e0207232.
19. Rana S, Rogers K, Lee T, Reed D, Biggs C. Dosimetric impact of Acuros XB dose calculation algorithm in prostate cancer treatment using RapidArc. *J Cancer Res Ther*. 2013;9(3):430–435.
20. Zifodya JM, Challens CH, Hsieh WL. From AAA to Acuros XB-clinical implications of selecting either Acuros XB dose-to-water or dose-to-medium. *Australas Phys Eng Sci Med*. 2016;39(2):431–439.
21. Guebert A, Conroy L, Weppler S, et al. Clinical implementation of AXB from AAA for breast: Plan quality and subvolume analysis. *J Appl Clin Med Phys*. 2018;19(3):243–250.
22. Fogliata A, Nicolini G, Clivio A, Vanetti E, Cozzi L. On the dosimetric impact of inhomogeneity management in the Acuros XB algorithm for breast treatment. *Radiat Oncol*. 2011;6:103.
23. Offersen BV, Boersma LJ, Kirkove C, et al. ESTRO consensus guideline on target volume delineation for elective radiation therapy of early stage breast cancer. *Radiother Oncol*. 2015;114(1):3–10.
24. Ulmer W, Harder D. A triple gaussian pencil beam model for photon beam treatment planning. *Z Med Phys*. 1995;5:25–30.
25. Ulmer W, Harder D. Applications of a triple gaussian pencil beam model for photon beam treatment planning. *Z Med Phys*. 1996;6:68–74.
26. Vassiliev ON, Wareing TA, McGhee J, Failla G, Salehpour MR, Mourtada F. Validation of a new grid-based Boltzmann equation solver for dose calculation in radiotherapy with photon beams. *Phys Med Biol*. 2010;55(3):581–598.
27. Heremans A, Verschakelen JA, Van fraeyenhoven L, Demedts M. Measurement of lung density by means of quantitative CT scanning. A study of correlations with pulmonary function tests. *Chest*. 1992;102(3):805–811.
28. International Commission on Radiation Units and Measurement. Prescribing, Recording, and Reporting Photon-Beam Intensity-Modulation Radiation Therapy (IMRT). Oxford: ICRU; 2010. ICRU Report 83.
29. Kumar L, Yadav G, Raman K, Bhushan M, Pal M. The dosimetric impact of different photon beam energy on RapidArc radiotherapy planning for cervix carcinoma. *J Med Phys*. 2015;40:207–213.
30. Kumar L, Yadav G, Samuvel KR, et al. Dosimetric influence of filtered and flattening filter free photon beam on rapid arc (RA) radiotherapy planning in case of cervix carcinoma. *Rep Pract Oncol Radiother*. 2017;22(1):10–18.
31. Hanley J, Debois MM, Mah D, et al. Deep inspiration breath-hold technique for lung tumors: The potential value of target immobilization and reduced lung density in dose escalation. *Int J Radiat Oncol Biol Phys*. 1999;45(3):603–611.
32. Hedin Emma, Bäck Anna, Chakarova Roumiana. Impact of lung density on the lung dose estimation for radiotherapy of breast cancer. *Phys Imaging Radiat Oncol*. 2017;3:5–10.
33. Kumar L, Yadav G, Kishore V, Bhushan M. Dosimetric validation of Acuros XB photon dose calculation algorithm on an indigenously fabricated low density heterogeneous phantom. *Radiat Prot Environ*. 2019;42:173–179.
34. Han T, Mikell J, Salehpour M, et al. Dosimetric comparison of AcurosXB deterministic radiation transportmethod with Monte Carlo and model-based convolution methods in heterogeneous media. *Med Phys*. 2011;38:2651–2664.
35. Blom Goldman U, Wennberg B, Svane G, Bylund H, Lind P. Reduction of radiation pneumonitis by V20-constraints in breast cancer. *Radiat Oncol*. 2010;5:99.
36. Marks LB, Bentzen SM, Deasy JO, et al. Radiation dose-volume effects in the lung. *Int J Radiat Oncol Biol Phys*. 2010;76(3 Suppl):S70–6.
37. Lind PA, Svane G, Gagliardi G, Svensson C. Abnormalities by pulmonary regions studied with computer tomography following local or localregional radiotherapy for breast cancer. *Int J Radiat Oncol Biol Phys*. 1999;43:489–496.

38. Rana S, Rogers K, Lee T, Reed D, Biggs C. Verification and dosimetric impact of acuros XB algorithm for stereotactic body radiation therapy (SBRT) and RapidArc planning for non-small-Cell lung Cancer (NSCLC) patients. *Int J Med Phys Clin Eng Radiat Oncol*. 2013;2(1):6–14.

39. Kathirvel M, Subramanian S, Clivio A, et al. Critical appraisal of the accuracy of Acuros-XB and Anisotropic Analytical Algorithm compared to measurement and calculations with the compass system in the delivery of RapidArc clinical plans. *Radiat Oncol*. 2013;8:140.